ResearchGate

See discussions, stats, and author profiles for this publication at: https://www.researchgate.net/publication/276356175

Cation Diffusivity and the Mixed Network Former Effect in Borosilicate Glasses

ARTICLE *in* THE JOURNAL OF PHYSICAL CHEMISTRY B · MAY 2015

Impact Factor: 3.3 · DOI: 10.1021/acs.jpcb.5b03520 · Source: PubMed

READS

17

3 AUTHORS, INCLUDING:

Morten M Smedskjaer

Aalborg University

79 PUBLICATIONS **790** CITATIONS

SEE PROFILE

Yuanzheng Yue

Aalborg University

209 PUBLICATIONS **2,715** CITATIONS

SEE PROFILE

Available from: Yuanzheng Yue
Retrieved on: 26 January 2016

THE JOURNAL OF PHYSICAL CHEMISTRY B

Article

pubs.acs.org/JPCB

Cation Diffusivity and the Mixed Network Former Effect in Borosilicate Glasses

Morten M. Smedskjaer,*[,†,‡] John C. Mauro,[‡] and Yuanzheng Yue[†]

[†]Department of Chemistry and Bioscience, Aalborg University, DK-9220 Aalborg, Denmark

[‡]Science and Technology Division, Corning Incorporated, Corning, New York 14831, United States

ABSTRACT: Understanding the structural origins of cationic diffusion processes in silicate glasses is important for high-tech applications of silicate glasses. For glasses with more than one network former, transport properties such as diffusivity are often nonlinear functions of the particular distribution of these network formers, a phenomenon known as the mixed network former effect. Here, we investigate the sodium−potassium interdiffusion ($\bar{D}_{Na-K}$) and the calcium inward diffusion (D_{Ca}) in soda lime borosilicate glasses with varying silica/borate ratio but constant modifier content. Indeed, the structural organization of borosilicate glasses results in a pronounced nonlinear composition dependence of $\bar{D}_{Na-K}$ and D_{Ca} (i.e., the mixed network former effect). Initial addition of B_2O_3 to the glass system results in a significant decrease in both diffusivities, whereas the change in diffusivity per mole of added B_2O_3 decreases with increasing B_2O_3 concentration. Besides the influences of water content and atomic packing degree, we find that 99% of the composition dependence of log $\bar{D}_{Na-K}$ can be ascribed to the change in concentration of tetrahedral boron groups. This indicates that the formation of $BO_{4/2}$ groups slows down diffusion processes of alkali and alkaline earth ions. Therefore, the mixed network former effect of the studied glass series is linked with the change of the concentration of tetrahedral boron groups, which is caused by the interactions between the different types of network formers.

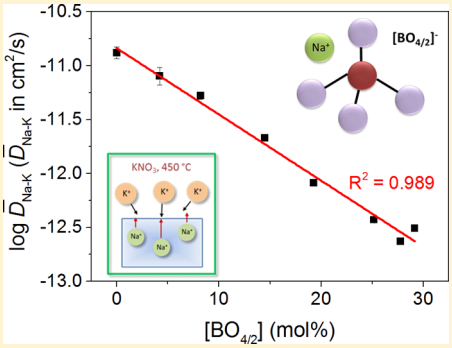

1. INTRODUCTION

The mixed network former effect (MNFE) is the nonadditive variation of a transport property as a function of the glass former composition at fixed modifier content.[1−3] The MNFE has been found in various mixed network former systems, including SiO_2−B_2O_3,[4−10] SiO_2−TeO_2,[11] P_2O_5−B_2O_3,[12,13] P_2O_5−TeO_2,[14,15] B_2O_3−TeO_2,[16,17] B_2O_3−V_2O_5,[18] MoO_3−B_2O_3,[19] MoO_3−P_2O_5,[20] MoO_3−TeO_2,[21] B_2S_3−P_2S_5,[22] GeO_2−P_2O_5,[23] GeO_2−GeS_2,[24] and GeS_2−SiS_2.[25] The effect has been observed as both maxima and minima in the transport property when one network former is replaced by another one. However, it is not a universal phenomenon in all mixed network former systems.[26] The MNFE should have a fundamental structural origin, but the detailed understanding of it is still lacking due to the complicated noncrystalline structure of multicomponent glasses.

Of the glass systems mentioned above, borosilicates glasses are technologically the most important ones. For example, alkali borosilicates have been applied for decades as thermal shock-resistant glasses (e.g., Pyrex),[27] and alkaline earth borosilicate glasses are used as substrate glasses for liquid crystal displays (e.g., EAGLE XG).[28] In borosilicate glasses, the mixing of silicon and boron structural units can be used to control and design the physical and chemical properties of these glasses. From a scientific perspective, the mixing of the structural units in borosilicates constitutes a major challenge due to the variety of possible structural groups in addition to the coordination change of boron with addition of network modifier ions (i.e., alkali or alkaline earth ions). That is, the initial addition of network modifier ions affects properties differently compared to further additions of these same modifiers. In detail, glassy B_2O_3 consists of corner-sharing $BO_{3/2}$ triangles (B^3), a large fraction of which combine to form three-membered boroxol ring units.[29−34] Upon addition of alkali or alkaline earth oxide to B_2O_3, there are two possibilities: (a) creation of a nonbridging oxygen (NBO), rupturing the linkage between two trigonally coordinated B^3 groups, or (b) conversion of boron from three-coordinated (trigonal boron, B^3) to a four-coordinated (tetrahedral boron, B^4) state without the creation of a NBO.[35]

Understanding the structural foundation of the composition and temperature dependence of conductivity and diffusion in borosilicate glasses is thus a major challenge. However, it is an important one, since tailoring of the alkali diffusivity in borosilicate glasses is crucial for recent high-tech applications of these glasses.[36−39] As recently reviewed by Wu et al.,[9] several studies have been conducted with respect to the transport properties of primarily sodium borosilicate glasses.[4−9,40−45] The general conclusion from these studies is that sodium diffusivity strongly decreases with increasing B_2O_3 content. However, since several factors (e.g., changes in water content and free volume) can contribute to the observed composition depend-

Received: April 12, 2015
Revised: May 14, 2015
Published: May 15, 2015

ACS Publications © 2015 American Chemical Society

DOI: 10.1021/acs.jpcb.5b03520
J. Phys. Chem. B 2015, 119, 7106−7115

Table 1. Analyzed Compositions and Selected Properties of the Investigated Glasses[a]

	chemical composition (mol %)									
glass ID	SiO_2	B_2O_3	Na_2O	CaO	Fe_2O_3	ρ (g/cm^3)	APF	T_g (K)	N_4 (at. %)	$[Fe^{3+}]/[Fe_{tot}]$ (at. %)
74B	0.0	73.1	15.2	10.7	1.0	2.344	0.569	771	39.9	93
62B-12Si	12.5	61.3	14.9	10.2	1.1	2.417	0.571	780	45.3	92
50B-24Si	23.1	51.5	14.2	10.2	1.0	2.490	0.575	792	48.9	91
37B-37Si	37.9	36.0	15.3	9.9	0.9	2.539	0.562	812	53.5	87
24B-50Si	52.1	22.1	14.0	10.8	1.0	2.581	0.547	826	65.5	87
12B-62Si	63.4	10.8	14.3	10.5	1.0	2.587	0.529	831	75.8	82
6B-68Si	69.1	5.2	14.8	9.9	1.0	2.570	0.516	829	80.8	78
74Si	75.3	0.0	13.9	9.7	1.1	2.530	0.499	817	n/a	79

[a]The fraction of four-coordinated to total boron (N_4) was determined using ^{11}B MAS NMR spectroscopy on analogous iron-free versions of these glasses.[46]

ence, it remains unclear to which extent glass structure variations are responsible for this dependence.[8−10]

We have recently performed a detailed structural and topological analysis of a series of soda lime borosilicate glasses, covering the extremes from pure borate to pure silicate end members at fixed Na_2O and CaO contents of 15 and 10 mol %, respectively.[46] We have derived a two-state statistical mechanical model of boron speciation in which addition of network modifiers leads to a competition between the formation of NBO and the conversion of boron from trigonal to tetrahedral configuration. Using this model, we have also derived a detailed topological representation[47,48] of alkali−alkaline earth-borosilicate glasses that enables quantitatively accurate predictions of various glass properties.[46] Here, we investigate the composition dependence of both sodium and calcium diffusion in this same series of glasses. By building on the knowledge obtained in our previous work, we aim at gaining deeper insights into the structural origins of the MNFE. Furthermore, this series of glasses allows us to investigate the diffusivity in three different structural regimes: (i) Na^+ and Ca^{2+} to convert boron from trigonal to tetrahedral configuration; (ii) Na^+ and Ca^{2+} to form NBOs on trigonal boron; and (iii) Na^+ and Ca^{2+} to form NBOs on tetrahedral silicon.

To our knowledge, all previous studies on diffusivity in mixed borosilicate glasses have focused on alkali diffusivity only. Here, we study the diffusivities of both sodium and calcium ions as a function of $[SiO_2]/[B_2O_3]$ ratio by using two different approaches. The first one is based on a K^+-for-Na^+ ion exchange process that occurs between the $Na_2O-CaO-B_2O_3-SiO_2$ glass and a molten KNO_3 bath.[36,37,49] By determining the penetration depth of the potassium ions into the glass, the effective interdiffusion coefficient ($\bar{D}_{Na-K}$) between Na^+ and K^+ can be obtained. Because of the slower movement of the larger potassium ions, the value of $\bar{D}_{Na-K}$ is generally lower than the sodium self-diffusion coefficient. Despite these differences in the absolute values of diffusion coefficients, good agreement between the composition dependences of alkali tracer diffusion coefficients and interdiffusion coefficients has been reported.[49,50] The second approach is based on the inward diffusion of cations from the glass surface into the interior of the glass that occurs upon thermal reduction of e.g., Fe^{3+} to Fe^{2+}.[51−53] The inward diffusion of mobile cations takes place in order to charge balance the outward flux of electron holes hopping from Fe^{3+} to Fe^{2+},[54,55] which occurs during thermal reduction. To study the inward diffusion, we have therefore prepared borosilicate glasses doped with 1 mol % Fe_2O_3. The inward diffusivities are calculated based on the surface depletion depth of the cations and the reduction time.[51] Tracer diffusion coefficients and inward diffusivities of alkaline earth ions have been reported to match well.[56,57]

In this work, we therefore prepare a series of iron-doped borosilicate glasses with the following compositions (in mol %): $(74-x)SiO_2-xB_2O_3-15Na_2O-10CaO-1Fe_2O_3$, where x = 0, 6, 12, 24, 37, 50, 62, and 74 (Table 1). By holding the amount of modifier constant, the possibility that diffusivity changes due a difference in the number of mobile cations is eliminated. We determine the density (ρ), glass transition temperature (T_g), iron redox state, and water content of the glasses prior to any diffusion experiments. In addition to the structural analyses already performed,[46] these measurements are useful for understanding the composition dependence of diffusion. We determine $\bar{D}_{Na-K}$ by ion exchange experiments in a molten KNO_3 bath and subsequent characterization of the refractive index profile at the surface. The calcium inward diffusivities of the samples under the H_2/N_2 (1/99 v/v) atmosphere are determined by measuring the elemental concentration profiles in the surface layer using secondary neutral mass spectroscopy (SNMS).

2. EXPERIMENTAL SECTION

2.1. Sample Preparation. The iron-doped borosilicate glasses were prepared from analytical reagent-grade H_3BO_3 (Sigma-Aldrich, ≥99.5%), SiO_2 (Sigma-Aldrich, purum p.a.), Na_2CO_3 (Merck, ≥99.9%), $CaCO_3$ (Merck, ≥99.5%), and Fe_2O_3 (Aldrich, ≥99.9%) powders. The mixed batch materials were then melted and homogenized in covered $Pt_{90}Rh_{10}$ crucibles at a temperature T_h in an inductively heated furnace. T_h was varied between 1100 and 1500 °C, and the melting time varied between 1 and 3 h depending on the level of silica. As shown in Table 1, the chemical composition analysis using wet chemistry reveals that the glasses are within 1−2 mol % of the desired compositions. There was no evidence of phase separation in these glasses.

The obtained glasses were then annealed at their respective T_g (see section 2.2) for 2 h to ensure uniform thermal histories. This is important due to the well-known thermal history dependence of diffusivity.[58,59] The glass samples were then cut to various dimensions depending on the experimental technique. Grinding and polishing were performed using a six-step procedure with SiC paper, followed by polishing with 3 μm diamond suspension. To prevent the chemical attack of water during grinding, ethanol (96 vol %) was used as grinding media. Moreover, all samples were kept in glass or plastic containers with desiccant.

2.2. Density and DSC Measurements. The free volume of the glass network structure influences the ease of cationic

DOI: 10.1021/acs.jpcb.5b03520
J. Phys. Chem. B 2015, 119, 7106−7115

diffusion processes. For low free volume or high atomic packing fraction, a high mechanical strain is imposed upon ionic transport, which generally lowers the diffusivity. In order to characterize the free volume of the network, we have measured the density of the annealed glasses. Density determination was carried out using the Archimedes' method by first weighing the sample in air and then weighing it when suspended in high-purity ethanol at room temperature (~21 °C).

The glass transition temperatures of the as-prepared glasses were determined calorimetrically using a differential scanning calorimetry (DSC) instrument (STA 449C Jupiter, Netzsch). The measurements were conducted in a purged argon atmosphere (40 mL/min). The isobaric heat capacity (C_p) curve for each measurement was calculated relative to the C_p curve of a sapphire reference material of comparable mass. The samples were subjected to two runs of DSC upscans and downscans at 10 K/min. Since the recorded heat flow of the first upscan reflects the enthalpy response of a sample with the unknown as-prepared thermal history, we determine T_g from the second upscan that reflects the enthalpy response of a sample with a well-defined thermal history. T_g is defined as the crossing point of the extrapolated straight line of the glass C_p curve before the transition zone with the tangent at the inflection point of the sharp rise curve of C_p in the transition zone.

2.3. Initial Water Content. Since the presence of water in glasses can slow down ionic transport processes[60−62] and B_2O_3-containing glasses are hygroscopic, we have determined the initial water content of the samples. For relatively low water concentrations, all water in silicate glass is present in the form of structurally bonded hydroxyl groups.[63] The vibrational stretching modes of these groups can be detected using Fourier transform infrared (FT-IR) spectroscopy, since Si−OH and B−OH absorption bands are present around 3500 cm^{-1}. With an increase in the water content of the sample, the intensities of these bands increase proportionally.

The samples used for these analyses were ground and polished to a uniform thickness of 1.0 mm. The FT-IR spectra were acquired using a Nicolet Nexus 670 FTIR spectrometer (Thermo Scientific) equipped with KBr beamsplitter and a DTGS detector. The absorption spectra were collected in the wavenumber region from 400 to 4000 cm^{-1} using air as reference. Data were averaged over 64 scans.

2.4. Iron Redox State. To investigate the composition dependence of inward diffusion processes, we must determine the initial iron redox ratio of the glasses. This is because the redox state impacts the extent of Fe^{3+} reduction and hence that of the sodium and calcium inward diffusion.[51] We first attempted to perform quantitative ^{57}Fe Mössbauer spectroscopy measurements, but the iron content of the samples was too low to obtain statistically reliable spectra. Instead, we estimated the iron redox ratio by thermogravimetry (TG) measurements in air on a simultaneous thermal analyzer (STA 449C Jupiter, Netzsch). As described in detail elsewhere,[64,65] the recorded weight increase during heating due to oxygen incorporation (i.e., oxidation of Fe^{2+}) was determined and used to estimate the $[Fe^{3+}]/[Fe_{tot}]$ ratio, where $[Fe_{tot}] = [Fe^{2+}] + [Fe^{3+}]$. Good agreement has been found between redox ratios obtained from this TG method and Mössbauer spectroscopy measurements.[64,65] The error in determining $[Fe^{3+}]/[Fe_{tot}]$ using the TG method is estimated to be around ±5%.

2.5. Diffusion Experiments. For ion exchange experiments, the annealed glasses were cut into square slides (10 × 10 × 1 mm^3), and both faces were polished. These samples were then immersed into a molten salt bath of technical grade KNO_3 at 450 °C for 32 h. The penetration depth of the potassium ions was determined in order to obtain the effective interdiffusion coefficient $\bar{D}_{Na-K}$. The exchange between Na^+ and K^+ gives the glass surface a higher refractive index than the interior, which is utilized in an FSM-6000 instrument (Orihara) to measure the saturation depth of the refraction index profile, which corresponds to the diffusion depth of potassium.[66] We performed a total of eight FSM measurements on each sample (using four 90° rotations per face).

Inward diffusion experiments were performed on cylindrical samples (10 mm diameter; 3 mm thickness) with one polished face. These samples were heat-treated in a H_2/N_2 (1/99) atmosphere at 500 °C for 8 h. Five selected glasses (74B, 62B-12Si, 37B-37Si, 12B-62Si, and 74Si) were also heat-treated for 8 h at 450, 475, and 540 °C in order to study the temperature dependence of diffusivity. The inward diffusion depths of calcium were then determined as the depletion depth of calcium in the surface region. This was done by measuring the elemental concentration profiles in the surface layer by electron gas SNMS measurements performed on an INA-X instrument (SPECS) equipped with a QMG 422 quadrupole mass spectrometer (Balzers Instruments) and a SEM SEV18 amplifier (Phillips). An area of 8 mm diameter was analyzed by sputtering using Kr plasma with energy of 350 eV. The time dependences of the sputter profiles were converted into depth dependencies by measuring the depth of the sputter crater at 12 different directions on the same sample with a P1 profilometer (Tencor).

3. RESULTS

3.1. Network Structure and Atomic Packing. Figure 1 shows the composition dependence of the glass transition temperature of the iron-containing soda lime borosilicate glasses. T_g first increases with increasing $[SiO_2]/([SiO_2] + [B_2O_3])$ ratio and then slightly decreases when the ratio is above ~0.85. Qualitatively, this is explained by an increasing number of the rigid constraints around silicon atoms compared to those around boron. On the other hand, the presence of B_2O_3 causes some of the modifiers to be used for charge-balancing four-coordinated boron and thus not creating NBOs. A high concentration of NBOs corresponds to a lower network connectivity, which generally results in a lower glass transition

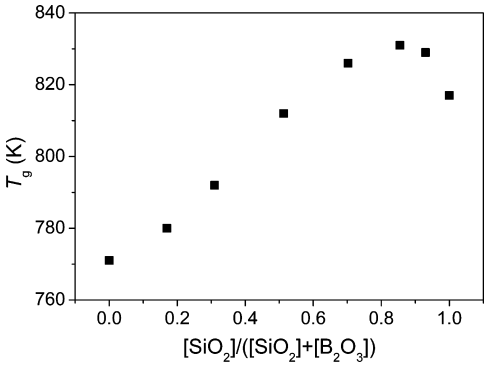

Figure 1. Composition dependence of the glass transition temperature (T_g). T_g has been determined using DSC at a heating/cooling rate of 10 K/min. The error in T_g associated with this method is generally 2−3 K.

DOI: 10.1021/acs.jpcb.5b03520
J. Phys. Chem. B 2015, 119, 7106−7115

temperature. This is why T_g increases with increasing concentration of B_2O_3 in the region of higher $[SiO_2]/([SiO_2] + [B_2O_3])$ ratios, where some modifiers are utilized for charge-balancing boron instead of creating NBOs. A quantitatively accurate prediction of $T_g(x)$ is presented elsewhere.[46]

The composition dependence of T_g is thus a reflection of the structural change of the glassy network with composition. Such knowledge is important for understanding composition and temperature dependence of diffusion in glass. It is also important to obtain information on the free volume in the glass structure that is available to the network modifiers for diffusion. This quantity can be estimated by first measuring the density of the glass samples (Figure 2a). Based on the density,

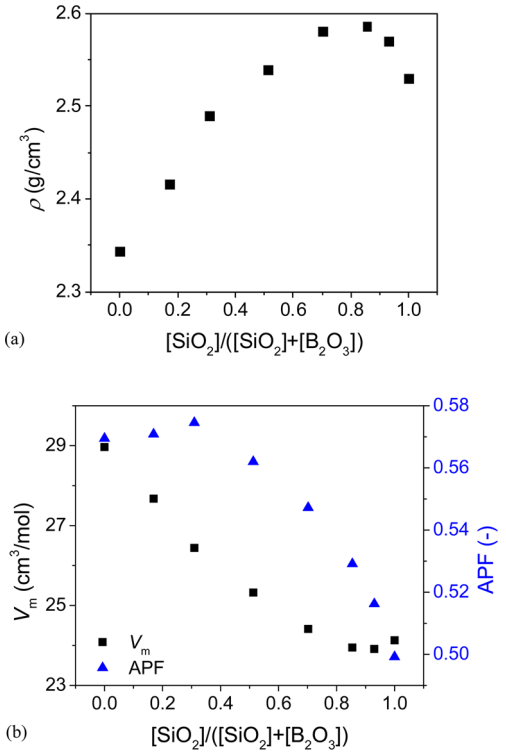

Figure 2. (a) Composition dependence of the glass density (ρ) of the investigated glasses. (b) Composition dependence of molar volume (V_m) and atomic packing factor (APF) of the glasses. APF is calculated using eq 1 from densities, compositions, and ionic radii.

the atomic packing factor (APF) can be calculated. APF is the ratio between the minimum theoretical volume occupied by the ions and the corresponding molar volume of the glass. Hence, the APF gives information about the free volume in the glass available for diffusion and not simply the overall molar volume (V_m) of the glass. APF is calculated as[67]

$$\mathrm{APF} = \rho \frac{\sum f_i V_i}{\sum f_i M_i} \tag{1}$$

for the ith constituent with the formula A_xB_y. f_i is the molar fraction, M_i the molar mass, and $V_i = (4/3)\pi N_a(x r_A^3 + y r_B^3)$ the theoretical volume, where r_A and r_B are the ionic radii and N_a is Avogadro's number. We have calculated APF by using the effective ionic radii given by Shannon[68] (Table 1). Figure 2b illustrates the composition dependence of both molar volume ($V_m = M/\rho$) and APF. While V_m gradually decreases with increasing silica content, APF is unaffected by addition of B_2O_3 to the soda lime silicate glass until $[B_2O_3] \sim 10$ mol % and then decreases with further additions of B_2O_3. Hence, the network structure of the borate end-member is significantly more closely packed than the silicate end-member, providing less open space for the modifiers to diffuse.

3.2. Water Content. The water content of the glasses is estimated using FT-IR spectroscopy to determine the intensity of the Si−OH and B−OH stretching bands. We do this by following the procedure for sodium borosilicate glasses.[8,9,69] The analysis is based on the Beer−Lambert law, which relates the concentration (by weight) of water in the glass (c_{H_2O}) to the absorbance of the IR beam through the glass (A):

$$c_{H_2O} = \frac{AM_{H_2O}}{\varepsilon_{H_2O}\Delta x \rho} = \frac{AM_{H_2O}}{2\varepsilon_{OH}\Delta x \rho} \tag{2}$$

where M_{H_2O} is the molar mass of H_2O, ε_{H_2O} is the molar absorption coefficient related to the overall concentration of water in the glass, and Δx is the sample thickness. The molar absorption coefficient of OH groups (ε_{OH}) is approximately equal to one-half of ε_{H_2O}, assuming that all water is present in the form of OH groups.[8,9] We do not know the actual values of ε_{OH} for the studied glasses, but studies have shown that variations of ε_{OH} are within 1 order of magnitude for various silicate glasses.[70] Following Wu et al.,[8,9] we therefore reorganize eq 2:

$$c_{H_2O}\varepsilon_{OH} = \frac{AM_{H_2O}}{2\Delta x \rho} \tag{3}$$

Assuming ε_{OH} to be a constant, variations in water concentrations are proportional to the right-hand side of eq 3. Figure 3 shows the values of $c_{H_2O}\varepsilon_{OH}$ as a function of

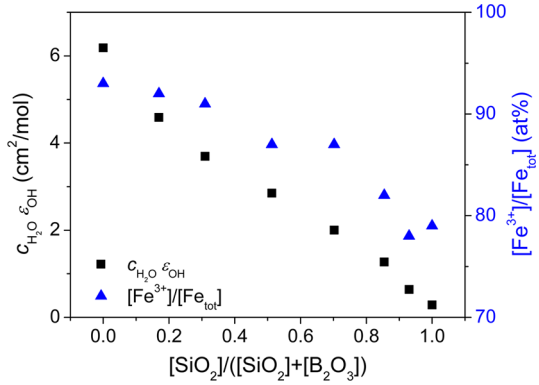

Figure 3. Initial water contents and iron redox ratio of the borosilicate glasses. Water contents are expressed as the product of the mass fraction of water in the glass (c_{H_2O}) and the molar absorption coefficient of OH groups (ε_{OH}), and they were determined using transmission FT-IR spectroscopy. Iron redox ratios are expressed as $[Fe^{3+}]/[Fe_{tot}]$, and they were estimated from thermogravimetric analyses.

composition. Because of the more hygroscopic nature of borate in comparison to silicate glasses, it is not surprising to find that the water content decreases with increasing $[SiO_2]/([SiO_2] + [B_2O_3])$ ratio.

3.3. Iron Redox State. Quantifying the redox state of iron in the glasses is important for two reasons. First, Fe^{2+} and Fe^{3+} affect the alkali and alkaline earth diffusivity in different

DOI: 10.1021/acs.jpcb.5b03520
J. Phys. Chem. B 2015, 119, 7106−7115

manners due to the different structural roles of the two ions. Fe^{2+} acts as a modifier ion[71] and hence occupies the percolative channels in the glassy network that are used for diffusion.[72,73] Addition of Fe^{2+} to a silicate glass therefore decreases the diffusivity more than addition of Fe^{3+}.[49] Second, the spatial extent of the inward diffusion process depends on the initial redox state of iron, since the process is driven by the reduction of Fe^{3+} to Fe^{2+}.[51] The TG measurements performed in air reveal slight differences in the mass increase during heating among the different glasses; i.e., the $[Fe^{3+}]/[Fe_{tot}]$ ratio varies slightly with composition. The determined values of $[Fe^{3+}]/[Fe_{tot}]$ are stated in Table 1 and shown in Figure 3. We find that $[Fe^{3+}]/[Fe_{tot}]$ decreases with increasing $[SiO_2]/([SiO_2] + [B_2O_3])$ ratio. $[Fe^{3+}]/[Fe_{tot}]$ varies between 78 and 93 at. %.

3.4. Sodium−Potassium Interdiffusion. The sodium−potassium interdiffusion coefficient D_{Na-K} is given by the Nernst−Planck equation

$$D_{Na-K} = \frac{D_{Na}D_K}{D_{Na}N_{Na} + D_K N_K} \quad (4)$$

where D_i and N_i are the self-diffusion coefficient and fractional concentration of alkali ion i, respectively. However, D_{Na-K} varies with local composition (i.e., position of the surface diffusion profile) and time,[41] and we therefore define the effective interdiffusion coefficient ($\bar{D}_{Na-K}$) as a constant for a given diffusion profile. From the determined surface penetration depth of the potassium ions and the ion exchange time, we have calculated $\bar{D}_{Na-K}$ at 450 °C for the different glasses (Figure 4a). We find that $\bar{D}_{Na-K}$ strongly depends on the $[SiO_2]/[B_2O_3]$ ratio, with diffusion occurring much faster in the silica-rich glasses. To illustrate this more clearly, we have plotted the composition dependence of log $\bar{D}_{Na-K}$ in Figure 4b. This plot reveals a significant MNFE effect with a nonlinear relationship between the logarithmic diffusivities of the two end-member glasses. In fact, the lowest value of $\bar{D}_{Na-K}$ is found for the 62B-12Si glass. The difference between the measured values of log $\bar{D}_{Na-K}$ and the linear relationship (i.e., the degree of MNFE) is designated as Δ log $\bar{D}_{Na-K}$ and plotted as a function of composition in Figure 4c.

3.5. Calcium Inward Diffusion. The apparent calcium inward diffusivity (D_{Ca}) is calculated from the concentration depth profiles in the surface layers of glasses subjected to thermal reduction in H_2/N_2 (1/99). The measured profiles are qualitatively similar to those reported elsewhere.[49,56] Based on the calcium depletion depth and the reduction time, D_{Ca} is calculated.[51] Figures 5a and 5b illustrate the composition dependence of D_{Ca} and log D_{Ca}, respectively, at 500 °C. We find that the calcium diffusivity exhibits a qualitatively similar composition dependence to that of the alkali interdiffusivity; i.e., the calcium diffusion occurs significantly faster in the silica-rich glasses. However, the calcium diffusivity is a few orders of magnitude slower than the alkali interdiffusivity due to the charge difference.

For five selected glasses, we have analyzed the temperature dependence of the calcium inward diffusivity. In the studied temperature range (450−540 °C), an Arrhenius equation was used to fit the data

$$D_{Ca} = D_{Ca}^0 \exp\left(\frac{-\Delta E_{a,Ca}}{RT}\right) \quad (5)$$

where $\Delta E_{a,Ca}$ and D_{Ca}^0 are the activation energy and pre-exponential factor, respectively. Good agreement with the Arrhenius equation is found (Figure 6a). The composition dependence of the fitted values of $\Delta E_{a,Ca}$ is shown in Figure 6b. $\Delta E_{a,Ca}$ decreases form 196 ± 7 to 136 ± 7 kJ/mol when $[SiO_2]/([B_2O_3] + [SiO_2])$ increases from 0 to 1.

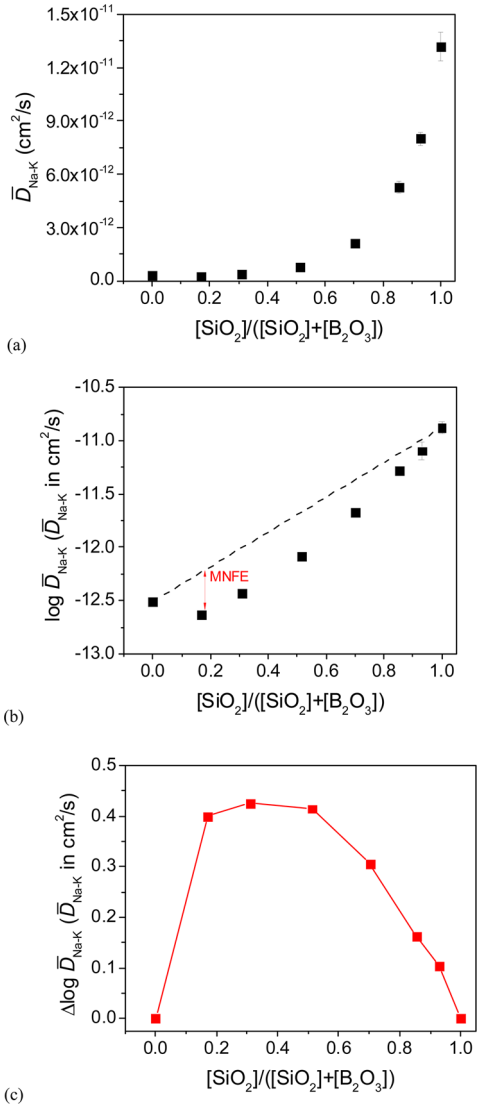

Figure 4. (a, b) Composition dependence of the K^+-for-Na^+ effective interdiffusion coefficient ($\bar{D}_{Na-K}$) as determined from isothermal ion exchange experiments at 450 °C plotted on (a) linear and (b) logarithmic scales. The error bars represent the standard deviation of the eight measurements on the same sample. (c) Composition dependence of the difference Δ log $\bar{D}_{Na-K}$ between measured values of log $\bar{D}_{Na-K}$ and those predicted assuming linearity between the two end-member glasses, i.e., the degree of the MNFE.

4. DISCUSSION

Several factors can influence the sodium and calcium diffusivities in the studied borosilicate glasses, including the structural role of the modifier cation, the free volume, and the presence of impurities. We have found that the concentration of OH groups increases with decreasing $[SiO_2]/([SiO_2] + [B_2O_3])$ ratio (Figure 3) and simultaneously the sodium and calcium diffusivities decrease (Figures 4 and 5). Previous studies have concluded that the presence of OH groups slows down ionic transport processes.[60−62] However, we do not know how large the influence of OH groups is on the cationic

DOI: 10.1021/acs.jpcb.5b03520
J. Phys. Chem. B 2015, 119, 7106−7115

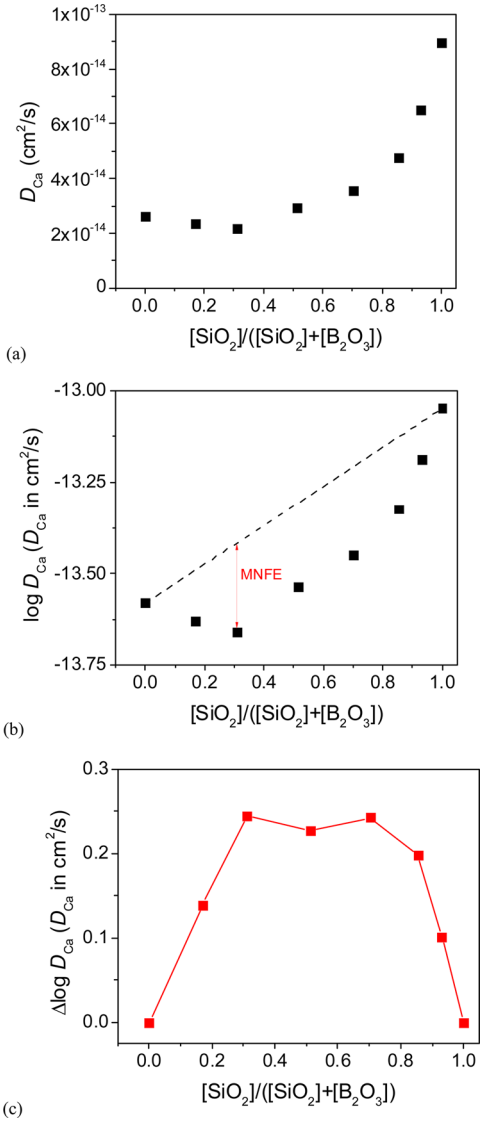

Figure 5. (a, b) Composition dependence of the apparent Ca^{2+} inward diffusivity (D_{Ca}) at 500 °C plotted on (a) linear and (b) logarithmic scales. (c) Composition dependence of the difference Δ log D_{Ca} between measured values of log D_{Ca} and those predicted assuming linearity between the two end-member glasses, i.e., the degree of the MNFE.

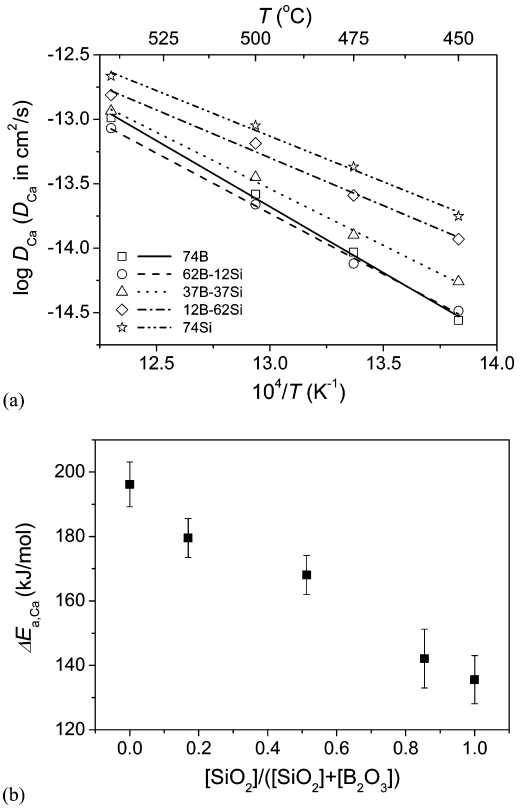

Figure 6. (a) Temperature dependence of the apparent Ca^{2+} inward diffusivity for five of the borosilicate glasses. The solid lines represent linear fits to the data using eq 5. (b) Composition dependence of the activation energy for calcium inward diffusion ($\Delta E_{a,Ca}$) obtained by fitting eq 5 to the experimental data in (a).

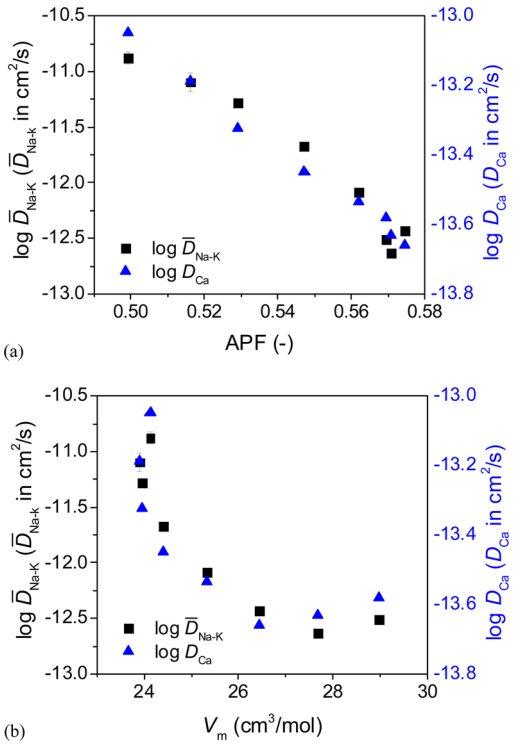

Figure 7. Dependences of the logarithmic sodium–potassium and calcium diffusivities on (a) atomic packing factor (APF) and (b) molar volume (V_m).

diffusivities for the glasses studied here. Similarly, we have found that the glass becomes more tightly packed with decreasing $[SiO_2]/([SiO_2] + [B_2O_3])$ ratio (Figure 2b). Hence, there is less space available for the modifying cations, which should also contribute to the lowering of diffusivities, even though the molar volume is actually increasing with decreasing $[SiO_2]/([SiO_2] + [B_2O_3])$. In Figures 7a and 7b we have plotted the logarithmic diffusivities against APF and V_m, respectively. The logarithmic diffusivities decrease linearly with increasing APF, whereas there is no clear dependence on V_m. This is because the free volume in the network structure (as reflected by APF) is more important for diffusivities than the overall molar volume of the glass.

Consequently, both the change in water content and atomic packing fractions contribute to the observed composition dependence of isothermal diffusivity. To further understand this composition dependence, it is also crucial to consider the

DOI: 10.1021/acs.jpcb.5b03520
J. Phys. Chem. B 2015, 119, 7106–7115

composition−structure relation of the glasses. In the silicate end-member composition, Na^+ and Ca^{2+} depolymerize the network by creating NBOs. In the borate end-member composition, essentially all Na^+ and Ca^{2+} ions are used for charge-balancing tetrahedral boron.[74] However, the structure of the glasses with compositions between the two end-members is not as simple; i.e., Na^+ and Ca^{2+} could convert boron from trigonal to tetrahedral configuration, form NBOs on trigonal boron, and/or form NBOs on tetrahedral silicon.

On the basis of our previous analysis,[46] we know that the fraction of modifiers creating NBOs increases gradually with increasing $[SiO_2]/([SiO_2] + [B_2O_3])$ ratio whereas the fraction of tetrahedral boron to total boron (N_4) gradually decreases (see Table 1). Moreover, we find that the diffusivities change most dramatically with composition near the silicate end-member. This suggests that the presence of $BO_{3/2}$ and $BO_{4/2}$ groups plays a major role in decreasing the diffusivities. To understand this behavior, we have plotted log $\bar{D}_{Na-K}$ vs $[BO_{4/2}]$ and $[BO_{3/2}]$ in Figure 8 using the analyzed compositions and

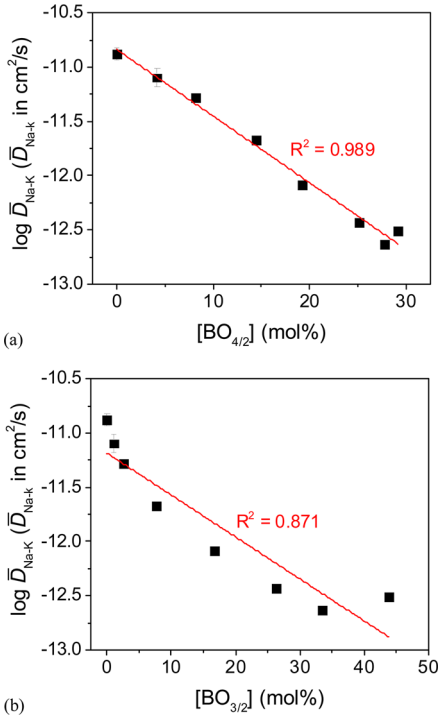

Figure 8. Effective interdiffusion coefficient ($\bar{D}_{Na-K}$) as a function of the concentration of (a) four-coordinated boron units and (b) three-coordinated boron units. $[BO_{4/2}]$ and $[BO_{3/2}]$ have been calculated based on the analyzed compositions and N_4 values from ^{11}B MAS NMR measurements on iron-free analogous glasses.[46] The solid lines represent linear fits to the data.

the measured N_4 values for iron-free analogous glasses.[46] The N_4 values calculated from iron-free glasses can be regarded as those of the iron-containing glasses with the same main composition, since we have previously found that the presence of 1 mol % Fe_2O_3 does not significantly change the boron speciation.[74] Here, we find that 99% of the variation in log $\bar{D}_{Na-K}$ can be explained by the variation in $BO_{4/2}$ concentration (Figure 8a), whereas only 87% of the variation can be explained by the change in $BO_{3/2}$ concentration (Figure 8b). This suggests that the tetrahedral boron groups are the main contributors to the lowering of diffusivities. This effect might be related to the fact that $BO_{4/2}$ units have been suggested to occur in corner-sharing pairs,[75,76] thus providing a "crowded" environment for diffusion. Another possible reason could simply be that the partial molar volume of $BO_{4/2}$ units is lower than that of the $BO_{3/2}$ units,[77] as reflected in the calculated atomic packing factor. Further studies are required to understand this effect in more details.

The composition dependence of the sodium−potassium interdiffusivity is qualitatively similar to that of the calcium inward diffusivity. This makes sense because two Na^+ ions behave similarly to one Ca^{2+} ion in the glass network. For example, there is no preference between Na^+ and Ca^{2+} to cause the boron coordination change.[74] If there were a preference, then the two types of ions should have displayed different compositions dependences of diffusivity. Furthermore, it is important to consider the initial redox of iron when interpreting the inward diffusivity data, since the inward diffusion process is driven by the reduction of Fe^{3+} to Fe^{2+}. $[Fe^{3+}]/[Fe_{tot}]$ decreases from around 93 to 79 at. % with increasing $[SiO_2]/([SiO_2] + [B_2O_3])$ (Table 1). Glass compositions with high optical basicity Λ_m (negative charge donating ability of oxygen) favor highly charged cations,[78−80] but Λ_m increases with increasing $[SiO_2]/([SiO_2] + [B_2O_3])$ ratio.[80] This composition dependence of $[Fe^{3+}]/[Fe_{tot}]$ must instead be attributed to an increase in the employed melt homogenization temperature with increasing silica content. However, the approximate 20 at. % variation in $[Fe^{3+}]/[Fe_{tot}]$ is too small to clarify the differences in diffusivities.[51] In addition, D_{Ca} increases with increasing $[SiO_2]/([SiO_2] + [B_2O_3])$, while the opposite would be expected if the variation in $[Fe^{3+}]/[Fe_{tot}]$ was responsible for the change. Therefore, the same structural effects mentioned above for $\bar{D}_{Na-K}$ should explain the isothermal composition dependence of D_{Ca}. These effect may also be responsible for the variation of the activation energy of calcium diffusion that decreases with increasing $[SiO_2]/([SiO_2] + [B_2O_3])$ ratio.

For sodium tracer diffusion in sodium borosilicate glasses, similar trends of the variation of diffusion activation energy with composition have been reported.[8,9] Likewise, according to Grandjean et al.,[44,45] the activation energy for electrical conductivity in sodium borosilicate glasses decreases with increasing $[SiO_2]/([SiO_2] + [B_2O_3])$ at fixed modifier content. In particular, the activation energy decreases linearly with the fraction of sodium ions bonded to NBOs on silicon and boron, i.e., the fraction of sodium ions not associated with tetrahedral boron.[44,45] They broke down the activation energy into two parts, viz., one for dissociation of Na−B^4 pair and another one for dissociation of Na−NBO pair with higher activation energy for the former. These findings agree well with our observation that most of the variation in diffusivity is caused by variations in the concentration of tetrahedral boron groups (Figure 8a). On the other hand, we note that in sodium borophosphate glasses $BO_{4/2}$ groups are favorable for ionic transport.[13] This implies again that understanding the detailed glass structure of the specific system is essential for clarifying the composition dependence of diffusivity.

5. CONCLUSIONS

We have investigated the composition dependence of isothermal sodium−potassium interdiffusion ($\bar{D}_{Na-K}$) and calcium inward diffusion (D_{Ca}) in mixed network soda lime borosilicate glasses. For both types of diffusion, we have observed a striking mixed network former effect; i.e., $\bar{D}_{Na-K}$ and

DOI: 10.1021/acs.jpcb.5b03520
J. Phys. Chem. B 2015, 119, 7106−7115

D_{Ca} reveal a strong nonlinear composition dependence. Both diffusivities decrease dramatically with initial addition of B_2O_3 to the silicate end-member composition, whereas additional addition of B_2O_3 causes a less pronounced decrease in diffusivities. The activation energy of calcium inward diffusion decreases with increasing $[SiO_2]/([SiO_2] + [B_2O_3])$ ratio. These variations are ascribed to differences in water content, degree of atomic packing, and structural role of network modifier among the different glasses. The structural effect plays a dominant role, and the concentration of four-coordinated boron groups can account for 99% of the composition dependence of log $\bar{D}_{Na-K}$.

AUTHOR INFORMATION

Corresponding Author

*E-mail: mos@bio.aau.dk (M.M.S.).

Notes

The authors declare no competing financial interest.

ACKNOWLEDGMENTS

We thank Joachim Deubener and Thomas Peter (Clausthal University of Technology) for SNMS measurements and Scott Aldrich (Corning Incorporated) for FT-IR measurements. We thank Marcel Potuzak (Corning Incorporated), Randall E. Youngman (Corning Incorporated), and Qiuju Zheng (Aalborg University) for helpful discussions.

REFERENCES

(1) Ingram, M. D. Ionic Conductivity in Glass. *Phys. Chem. Glasses* **1987**, *28*, 215−234.

(2) Martin, S. W. Ionic Conduction in Phosphate Glasses. *J. Am. Ceram. Soc.* **1991**, *74*, 1767−1784.

(3) Schuch, M.; Müller, C. R.; Maass, P.; Martin, S. W. Mixed Barrier Model for the Mixed Glass Former Effect in Ion Conducting Glasses. *Phys. Rev. Lett.* **2009**, 145902.

(4) Tatsumisago, M.; Minami, T.; Tanaka, M. Properties of Highly Ionic Conducting Li_4SiO_4-Li_3BO_3 Glasses Prepared by Rapid Quenching. *Glastech. Ber.* **1983**, *56*, 945−950.

(5) Tatsumisago, M.; Machida, N.; Minami, T. Mixed Anion Effect in Conductivity of Rapidly Quenched Li_4SiO_4-Li_3BO_3 Glasses. *J. Ceram. Soc. Jpn.* **1987**, *95*, 197−201.

(6) Kaps, C.; Schirrmeister, F.; Stefanski, P. J. On the Na^+ Self-Diffusion and Electrical Conductivity of Na_2O-B_2O_3-SiO_2 Glasses Derived from the $Na_2O{\cdot}2SiO_2$ Glass. *J. Non-Cryst. Solids* **1986**, *87*, 159−170.

(7) Kluvanek, P.; Klement, R.; Karacon, M. Investigation of the Conductivity of the Lithium Borosilicate Glass System. *J. Non-Cryst. Solids* **2007**, *353*, 2004−2007.

(8) Wu, X.; Dieckmann, R. Sodium Tracer Diffusion in Glasses of the Type $(Na_2O)_{0.2}[(BO_{1.5})_x(SiO_2)_{1-x}]_{0.8}$. *J. Non-Cryst. Solids* **2011**, *357*, 2846−2856.

(9) Wu, X.; Varshneya, A. K.; Dieckmann, R. Sodium Tracer Diffusion in Glasses of the Type $(Na_2O)_{0.2}(B_2O_3)_y(SiO_2)_{0.8-y}$. *J. Non-Cryst. Solids* **2011**, *357*, 3661−3669.

(10) Wu, X.; Youngman, R. E.; Dieckmann, R. Sodium Tracer Diffusion and ^{11}B NMR Study of Glasses of the Type $(Na_2O)_{0.17}(B_2O_3)_x(SiO_2)_{0.83-x}$. *J. Non-Cryst. Solids* **2013**, *378*, 168−176.

(11) Rodrigues, A. C. M.; Keding, R.; Rüssel, C. Mixed Former Effect between TeO_2 and SiO_2 in the $Li_2O{\cdot}TeO_2{\cdot}SiO_2$ System. *J. Non-Cryst. Solids* **2000**, *273*, 53−58.

(12) Magistris, A.; Chiodelli, G.; Duclot, M. Silver Borophosphate Glasses: Ion Transport, Thermal Stability and Electrochemical Behaviour. *Solid State Ionics* **1983**, *9−10*, 611−615.

(13) Zielnok, D.; Eckert, H.; Cramer, C. Direct Correlation between Nonrandom Ion Hopping and Network Structure in Ion-Conducting Borophosphate Glasses. *Phys. Rev. Lett.* **2008**, *100*, 035901.

(14) Coppo, D.; Duclot, M. J.; Souquet, J. L. Silver Ionic Conductivity Enhancement by Network Former Mixed in Oxide-Based Glasses. *Solid State Ionics* **1996**, *90*, 111−115.

(15) Jayasinghe, G. D. L. K.; Bandaranayake, P. W. S. K.; Souquet, J. L. Mixed Former Effect in Sodium Phospho Tellurate Glasses. *Solid State Ionics* **1996**, *86−88*, 447−451.

(16) Chowdari, B. V. R.; Kumari, P. P. Synthesis and Characterization of Silver Borotellurite Glasses. *Solid State Ionics* **1996**, *86−88*, 521−526.

(17) Shaw, A.; Ghosh, A. Dynamics of Lithium Ions in Borotellurite Mixed Former Glasses: Correlation between the Characteristic Length Scales of Mobile Ions and Glass Network Structural Units. *J. Chem. Phys.* **2014**, *141*, 164504.

(18) Jamal, Md.; Venugopal, G.; Shareefuddin, Md.; Chary, M. N. Sodium Ion Conducting Glasses with Mixed Glass Formers NaI-Na_2O-V_2O_5-B_2O_3: Application to Solid State Battery. *Mater. Lett.* **1999**, *39*, 28−32.

(19) Agrawal, R. C.; Verma, M. L.; Gupta, R. K.; Kumar, R. Transport Property and Mixed Former Effect Studies on a New Fast Ag^+ Ion Conducting Glass System: $0.7[0.75AgI{:}0.25AgCl]{:}0.3[Ag_2O{:}\{xB_2O_3{:}(1-x)MoO_3\}]$. *J. Phys. D: Appl. Phys.* **2002**, *35*, 810−815.

(20) Deb, B.; Kabi, S.; Ghosh, A. Mixed Glass Former Effect in Silver Molybdophosphate and Borophosphate Glasses. *AIP Conf. Proc.* **2011**, *1349*, 519−520.

(21) Chowdari, B. V. R.; Kumari, P. P. Effect of Mixed Glass-Formers in $Ag_2O.MoO_3.TeO_2$ System. *J. Phys. Chem. Solids* **1997**, *58*, 515−525.

(22) Haynes, M. J.; Bischoff, C.; Kaufmann, T.; Martin, S. W. The Mixed Glass Former Effect on the Thermal and Volume Properties of $Na_2S-B_2S_3-P_2S_5$ glasses. *Phys. Chem. Glasses: Eur. J. Glass Sci. Technol., Part B* **2009**, *50*, 144−148.

(23) Behrends, F.; Eckert, H. Mixed Network Former Effects in Oxide Glasses: Structural Studies in the System $(M_2O)_{1/3}[(Ge_2O_4)_x(P_2O_5)_{1-x}]_{2/3}$ by Solid State NMR Spectroscopy. *J. Phys. Chem. C* **2014**, *118*, 10271−10283.

(24) Kim, Y.; Saienga, J.; Martin, S. W. Anomalous Ionic Conductivity Increase in Li_2S + GeS_2 + GeO_2 Glasses. *J. Phys. Chem. B* **2006**, *110*, 16318−16325.

(25) Deshpande, V. K.; Pradel, A.; Ribes, M. The Mixed Glass Former Effect in the Li_2S: SiS_2: GeS_2 System. *Mater. Res. Bull.* **1988**, *23*, 379−384.

(26) Christensen, R.; Byer, J.; Olson, G.; Martin, S. W.; Shu, X. The Mixed Glass Former Effect in Sodium Borophosphate Glass. *Am. Ceram. Soc. Bull.* **2011**, *90* (5), 19−22.

(27) Smedskjaer, M. M.; Youngman, R. E.; Mauro, J. C. Principles of Pyrex® Glass Chemistry: Structure−Property Relationships. *Appl. Phys. A: Mater. Sci. Process.* **2014**, *116*, 491−504.

(28) Ellison, A.; Cornejo, I. A. Glass Substrates for Liquid Crystal Displays. *Int. J. Appl. Glass Sci.* **2010**, *1*, 87−103.

(29) Jellison, G. E.; Panek, L. W.; Bray, P. J.; Rouse, G. B. Determinations of Structure and Bonding in Vitreous B_2O_3 by Means of B^{10}, B^{11}, and O^{17} NMR. *J. Chem. Phys.* **1977**, *66*, 802−812.

(30) Micoulaut, M.; Kerner, R.; dos Santos-Loff, D. M. Statistical Modelling of Structural and Thermodynamical Properties of Vitreous B_2O_3. *J. Phys.: Condens. Matter* **1995**, *7*, 8035−8052.

(31) Youngman, R. E.; Haubrich, S. T.; Zwanziger, J. W.; Janicke, M. T.; Chmelka, B. F. Short-and Intermediate-Range Structural Ordering in Glassy Boron Oxide. *Science* **1995**, *269*, 1416−1420.

(32) Youngman, R. E.; Zwanziger, J. W. Multiple Boron Sites in Borate Glass Detected with Dynamic Angle Spinning Nuclear Magnetic Resonance. *J. Non-Cryst. Solids* **1994**, *168*, 293−297.

(33) Hannon, A. C.; Grimley, D. I.; Hulme, R. A.; Wright, A. C.; Sinclair, R. N. Boroxol Groups in Vitreous Boron Oxide: New Evidence from Neutron Diffraction and Inelastic Neutron Scattering Studies. *J. Non-Cryst. Solids* **1994**, *177*, 299−316.

DOI: 10.1021/acs.jpcb.5b03520
J. Phys. Chem. B 2015, 119, 7106−7115

(34) Ferlat, G.; Charpentier, T.; Seitsonen, A. P.; Takada, A.; Lazzeri, M.; Cormier, L.; Calas, G.; Mauri, F. Boroxol Rings in Liquid and Vitreous B_2O_3 from First Principles. *Phys. Rev. Lett.* **2008**, *101*, 065504.
(35) Varshneya, A. K. *Fundamentals of Inorganic Glasses*, 2nd ed.; Society of Glass Technology: Sheffield, 2006.
(36) Varshneya, A. K. The Physics of Chemical Strengthening of Glass: Room for a New View. *J. Non-Cryst. Solids* **2010**, *356*, 2289−2294.
(37) Varshneya, A. K. Chemical Strengthening of Glass: Lessons Learned and Yet To Be Learned. *Int. J. Appl. Glass Sci.* **2010**, *1*, 131−142.
(38) Ishizuka, S.; Hommoto, H.; Kido, N.; Hashimoto, K.; Yamada, A.; Niki, S. Efficiency Enhancement of Cu(In,Ga)Se_2 Solar Cells Fabricated on Flexible Polyimide Substrates using Alkali-Silicate Glass Thin Layers. *Appl. Phys. Express* **2008**, *1*, 092303.
(39) Ishizuka, S.; Yamada, A.; Matsubara, K.; Fons, P.; Sakurai, K.; Niki, S. Development of High-Efficiency Flexible Cu(In,Ga)Se_2 Solar Cells: A Study of Alkali Doping Effects on CIS, CIGS, and CGS using Alkali-Silicate Glass Thin Layers. *Curr. Appl. Phys.* **2010**, *10*, S154−S156.
(40) Otto, K. Electrical Conductivity of SiO_2-B_2O_3 Glasses Containing Lithium or Sodium. *Phys. Chem. Glasses* **1966**, *7*, 29−37.
(41) Varshneya, A. K.; Milberg, M. E. Ion Exchange in Sodium Borosilicate Glasses. *J. Am. Ceram. Soc.* **1974**, *57*, 165−169.
(42) Ehrt, D.; Keding, R. Electrical Conductivity and Viscosity of Borosilicate Glasses and Melts. *Phys. Chem. Glass: Eur. J. Glass Sci. Technol., Part B* **2009**, *50*, 165−171.
(43) Catchings, R. M. Influence of Composition and Structure on the Ionic Conductivity of the Glass System Na_2O-B_2O_3-SiO_2. *J. Appl. Phys.* **1980**, *52*, 1116−1117.
(44) Grandjean, A.; Malki, M.; Simonnet, C. Effect of Composition on Ionic Transport in SiO_2−B_2O_3−Na_2O Glasses. *J. Non-Cryst. Solids* **2006**, *352*, 2731−2736.
(45) Grandjean, A.; Malki, M.; Montouillout, V.; Debruycker, F.; Massiot, D. Electrical Conductivity and ^{11}B NMR Studies of Sodium Borosilicate Glasses. *J. Non-Cryst. Solids* **2008**, *354*, 1664−1670.
(46) Smedskjaer, M. M.; Mauro, J. C.; Youngman, R. E.; Hogue, C. L.; Potuzak, M.; Yue, Y. Z. Topological Principles of Borosilicate Glass Chemistry. *J. Phys. Chem. B* **2011**, *115*, 12930−12946.
(47) Gupta, P. K.; Mauro, J. C. Composition Dependence of Glass Transition Temperature and Fragility. I. A Topological Model Incorporating Temperature-Dependent Constraints. *J. Chem. Phys.* **2009**, *130*, 094503.
(48) Mauro, J. C. Topological Constraint Theory of Glass. *Am. Ceram. Soc. Bull.* **2011**, *90* (4), 31−37.
(49) Smedskjaer, M. M.; Zheng, Q. J.; Mauro, J. C.; Potuzak, M.; Mørup, S.; Yue, Y. Z. Sodium Diffusion in Boroaluminosilicate Glasses. *J. Non-Cryst. Solids* **2011**, *357*, 3744−3750.
(50) Frischat, G. H.; Kirchmeyer, R. Relation Between Tracer Diffusion and Ion Exchange in Silicate Glasses. *J. Am. Ceram. Soc.* **1973**, *56*, 552.
(51) Smedskjaer, M. M.; Yue, Y. Z. Inward Cationic Diffusion in Glass. *J. Non-Cryst. Solids* **2009**, *355*, 908−912.
(52) Smedskjaer, M. M.; Deubener, J.; Yue, Y. Z. Inward Cationic Diffusion and Formation of Silica-Rich Surface Nanolayer of Glass. *Chem. Mater.* **2009**, *21*, 1242−1247.
(53) Smedskjaer, M. M.; Yue, Y. Z. Redox Reactions and Inward Cationic Diffusion in Glasses Caused by CO and H_2 Gases. *Solid State Ionics* **2009**, *180*, 1121−1124.
(54) Cook, G. B.; Cooper, R. F. Iron Concentration and the Physical Processes of Dynamic Oxidation in an Alkaline Earth Aluminosilicate Glass. *Am. Mineral.* **2000**, *85*, 397−406.
(55) Cochain, B.; Neuville, D. R.; de Ligny, D.; Malki, M.; Testemale, D.; Pinet, O.; Richet, P. Dynamics of Iron-Bearing Borosilicate Melts: Effects of Melt Structure and Composition on Viscosity, Electrical Conductivity and Kinetics of Redox Reactions. *J. Non-Cryst. Solids* **2013**, *373*−*374*, 18−27.
(56) Smedskjaer, M. M.; Yue, Y. Z. Inward and Outward Diffusion of Modifying Ions and its Impact on the Properties of Glasses and Glass-Ceramics. *Int. J. Appl. Glass Sci.* **2011**, *2*, 117−128.
(57) Everman, R. L. A.; Cooper, R. F. Internal Reduction of an Iron-Doped Magnesium Aluminosilicate Melt. *J. Am. Ceram. Soc.* **2003**, *86*, 487−494.
(58) Frischat, G. H.; Beier, W. Influence of Preparation Conditions on Diffusion in Glasses. *J. Non-Cryst. Solids* **1985**, *71*, 77−85.
(59) Mehrer, H. *Diffusion in Solids: Fundamentals, Methods, Materials, Diffusion-Controlled Processes*, 1st ed.; Springer-Verlag: Berlin, 2007.
(60) Tian, L.; Dieckmann, R.; Hui, C.-Y.; Couillard, J. G. Effect of Water Incorporation on the Diffusion of Sodium in an Alkaline-Earth Boroaluminosilicate Glass. *J. Non-Cryst. Solids* **2001**, *296*, 123−134.
(61) Tian, L.; Lu, H. X.; Dieckmann, R. Influence of Water on the Tracer Diffusion of Sodium in Glasses. *Phys. Chem. Chem. Phys.* **2003**, *5*, 2202−2211.
(62) Tian, L.; Dieckmann, R. Incorporation of Water into Glasses and its Influence on the Diffusion of Cations, Including the Creation of Diffusion Barriers. *J. Non-Cryst. Solids* **2006**, *352*, 679−689.
(63) Shelby, J. E. *Introduction to Glass Science and Technology*, 2nd ed.; The Royal Society of Chemistry: Cambridge, 2005.
(64) Kirkegaard, L. F.; Korsgaard, M.; Yue, Y. Z.; Mørup, S. Redox Behaviour of Iron Bearing Glass Fibres during Heat Treatment under Atmospheric Conditions. *Glass Sci. Technol.* **2005**, *78*, 1−6.
(65) Smedskjaer, M. M.; Yue, Y. Z.; Deubener, J.; Mørup, S. Impact of Cationic Diffusion on Properties of Iron-Bearing Glass Fibres. *Phys. Chem. Glasses: Eur. J. Glass Sci. Technol., Part B* **2010**, *51*, 271−280.
(66) Kishii, T. Surface Stress Measurement Using Optical Waveguide Effect of Chemically Tempered Glass. *J. Ceram. Soc. Jpn.* **1978**, *87*, 119−126.
(67) Rouxel, T. Elastic Properties and Short-to-Medium Range Order in Glasses. *J. Am. Ceram. Soc.* **2007**, *90*, 3019−3039.
(68) Shannon, R. D. Revised Effective Ionic Radii and Systematic Studies of Interatomic Distances in Halides and Chalcogenides. *Acta Crystallogr., Sect. A: Cryst. Phys., Diffr., Theor. Gen. Crystallogr.* **1976**, *32*, 751−767.
(69) Bandyopadhyai, A. K.; Jabra, R.; Phalippou, J. Association of OH groups with Boron and Silicon Atoms in SiO_2-B_2O_3 Glasses by Infrared Spectroscopy. *J. Mater. Sci. Lett.* **1989**, *8*, 1464−1467.
(70) Peuker, C.; Bessau, W.; Brzezinka, K. W.; Kohl, A.; Reinholz, U.; Geibler, H. IR and Rarnan Study of Calcium Alumino-Silicate Glasses of the Composition $xCaOxAl_2O_3.(100-2x)SiO_2$. *Glass Sci. Technol.* **2002**, *75*, 313−322.
(71) Mysen, B. O.; Richet, P. *Silicate Glasses and Melts − Properties and Structure*; Elsevier: Amsterdam, 2005.
(72) Greaves, G. N. EXAFS and the Structure of Glass. *J. Non-Cryst. Solids* **1985**, *71*, 203−217.
(73) Huang, C.; Cormack, A. N. The Structure of Sodium Silicate Glass. *J. Chem. Phys.* **1990**, *93*, 8180−8186.
(74) Smedskjaer, M. M.; Mauro, J. C.; Sen, S.; Yue, Y. Z. Quantitative Design of Glassy Materials using Temperature-Dependent Constraint Theory. *Chem. Mater.* **2010**, *22*, 5358−5365.
(75) Gupta, P. K. The Random-Pair Model of Four-Coordinated Borons in Alkali-Borate Glasses, Proceedings of the International Congress on Glass, New Delhi, 1986; pp 1−10.
(76) Mauro, J. C.; Gupta, P. K.; Loucks, R. J. Composition Dependence of Glass Transition Temperature and Fragility. II. A Topological Model of Alkali Borate Liquids. *J. Chem. Phys.* **2009**, *130*, 234503.
(77) Lower, N. P.; McRae, J. L.; Feller, H. A.; Betzen, A. R.; Kapoor, S.; Affatigato, M.; Feller, S. A. Physical Properties of Alkaline-Earth and Alkali Borate Glasses Prepared over an Extended Range of Compositions. *J. Non-Cryst. Solids* **2001**, *293*−*295*, 669−675.
(78) Duffy, J. A.; Ingram, M. D. Establishment of an Optical Scale for Lewis Basicity in Inorganic Oxyacids, Molten Salts, and Glasses. *J. Am. Chem. Soc.* **1971**, *93*, 6448−6454.
(79) Duffy, J. A.; Ingram, M. D. An Interpretation of Glass Chemistry in terms of the Optical Basicity Concept. *J. Non-Cryst. Solids* **1976**, *21*, 373−410.

DOI: 10.1021/acs.jpcb.5b03520
J. Phys. Chem. B 2015, 119, 7106−7115

(80) Duffy, J. A. A Review of Optical Basicity and its Applications to Oxidic Systems. *Geochim. Cosmochim. Acta* **1993**, *57*, 3961−3970.

DOI: 10.1021/acs.jpcb.5b03520
J. Phys. Chem. B 2015, 119, 7106−7115